Supplementary Materials

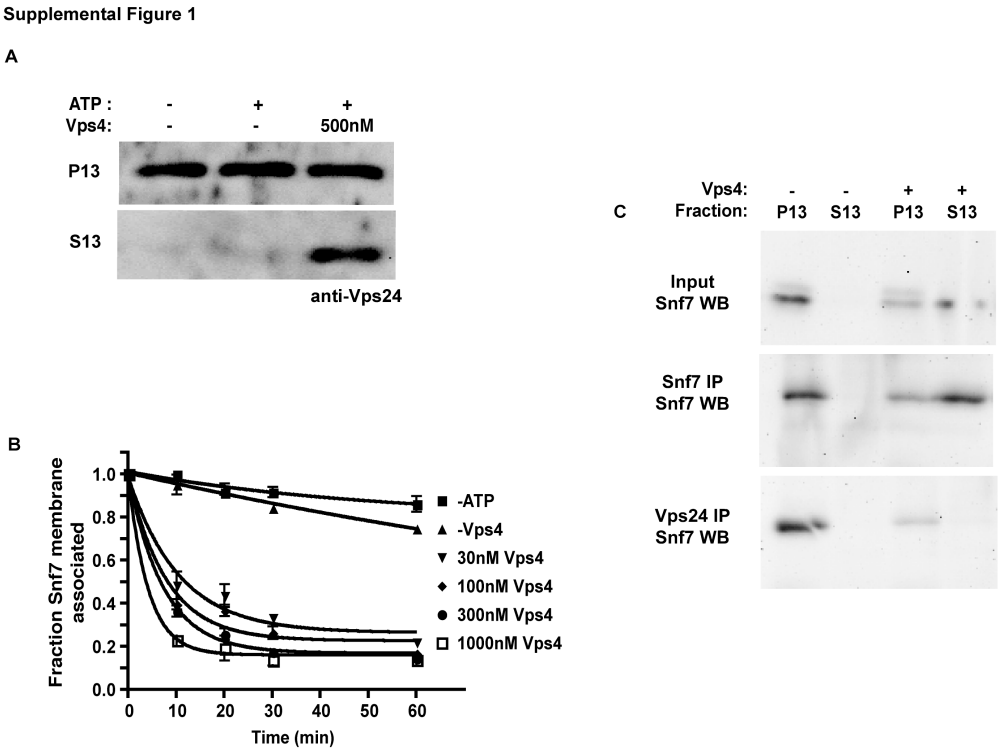

Supplementary Figure 1. Additional characterization of Vps4-mediated ESCRT-III disassembly in vitro. (**A**) ESCRT-III release reactions were initiated with 10 OD_{600} equivalents of resuspended P13 membranes, generated from *vps4*Δ cells expressing Vps20-HA (as in Figure 1C, D), in the presence (+) or absence (-) of 1mM ATP and an ATP regeneration system (ATP) and 500nM Vps4. Following a 30 minute incubation at 30°, samples were subjected to centrifugation at 13,000 g to separate the membrane-associated (P13) and soluble (S13) material. Western blotting with Vps24 antiserum was performed. Quantitation of Snf7 release from the membrane under these conditions is presented in Figure 1E. (**B**) ESCRT-III membrane release reactions were initiated with 0.5 OD_{600} equivalents of resuspended P13 membranes, as in Figure 1A, with increasing concentrations of Vps4 (30nM, 100nM, 300nM, and 1μM). Following incubations for 10, 20, 30 or 60 minutes at 30°, samples were subjected to centrifugation at 13,000 g (at 4°) to separate the membrane-associated (P13) and soluble (S13) material. Western blotting with Snf7 antiserum was performed, and the fraction of Snf7 remaining membrane associated is presented. (**C**) Co-immunoprecipitation of Snf7 with Vps24 antiserum. ESCRT-III release reactions (10 OD_{600} equivalents) were performed with 500nM Vps4. Following a 30 minute incubation at 30°, samples were subjected to centrifugation at 13,000 g to separate the membrane-associated (P13) and soluble (S13) material. P13-associated material was subjected to TritonX-100 extraction, and then both

S13 and extracted P13 material were subjected to immunoprecipitation with Snf7 or Vps24 antiserum. The P13 input material represents TritonX-100 extracted sample. Western blotting with Snf7 antiserum was performed. Snf7 release into the S13 corresponds to a reduction in immunoprecipitation with Vps24 antiserum, consistent with Snf7 release from the membrane correlating with ESCRT-III dissociation.

Supplementary Figure 2. Additional characterization of ESCRT-III subunit dependence of Vps4-mediated ESCRT-III disassembly. (**A**) Examination of Snf7 levels in resuspended P13 membranes utilized in these assays. All strains lack Vps4 (*vps4*Δ) and the vacuolar protease Proteinase A (*pep4*Δ). Western blotting for Pep12 was performed as a loading control. (**B**) ESCRT-III containing membranes were generated from yeast lacking the core ESCRT-III subunit Vps24 and the accessory ESCRT-III subunits Did2 (blue). These membranes (0.5 OD_{600} equivalent) were incubated with ATP and 100nM or 1μM Vps4, and the fraction of Snf7 remaining membrane associated was determined, as in **Figure 1**.

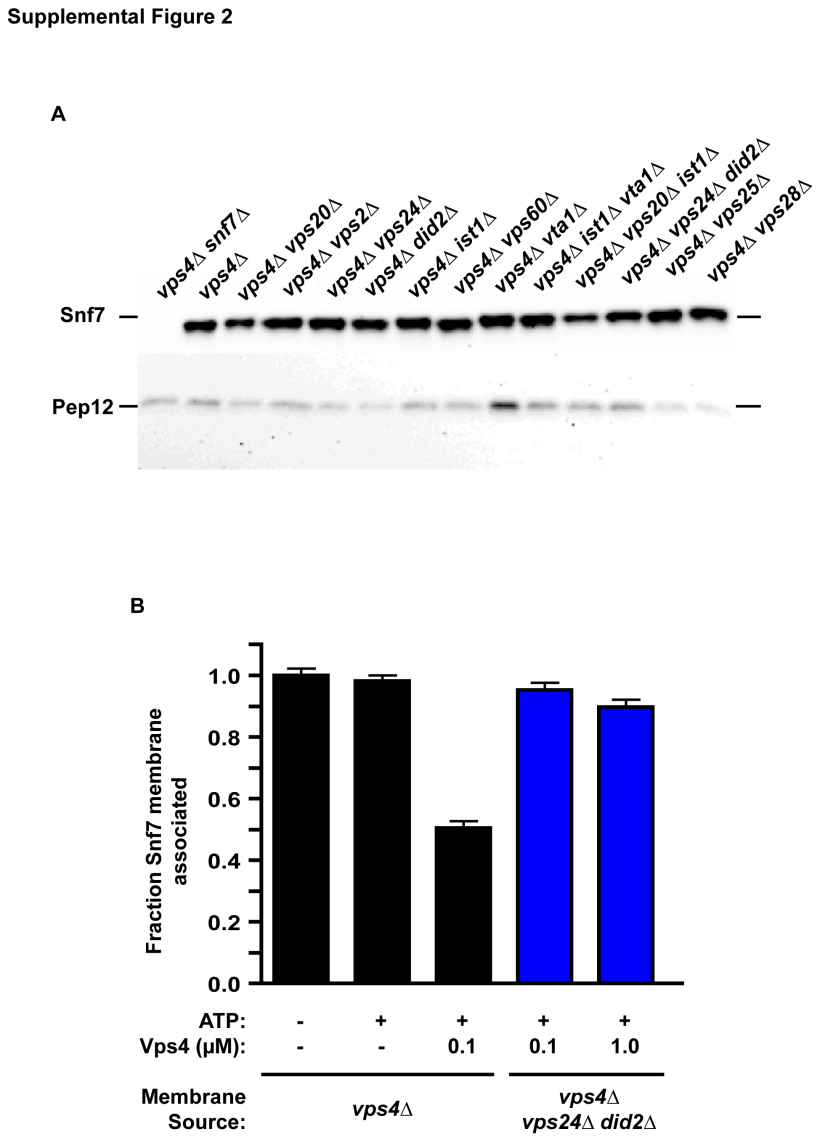

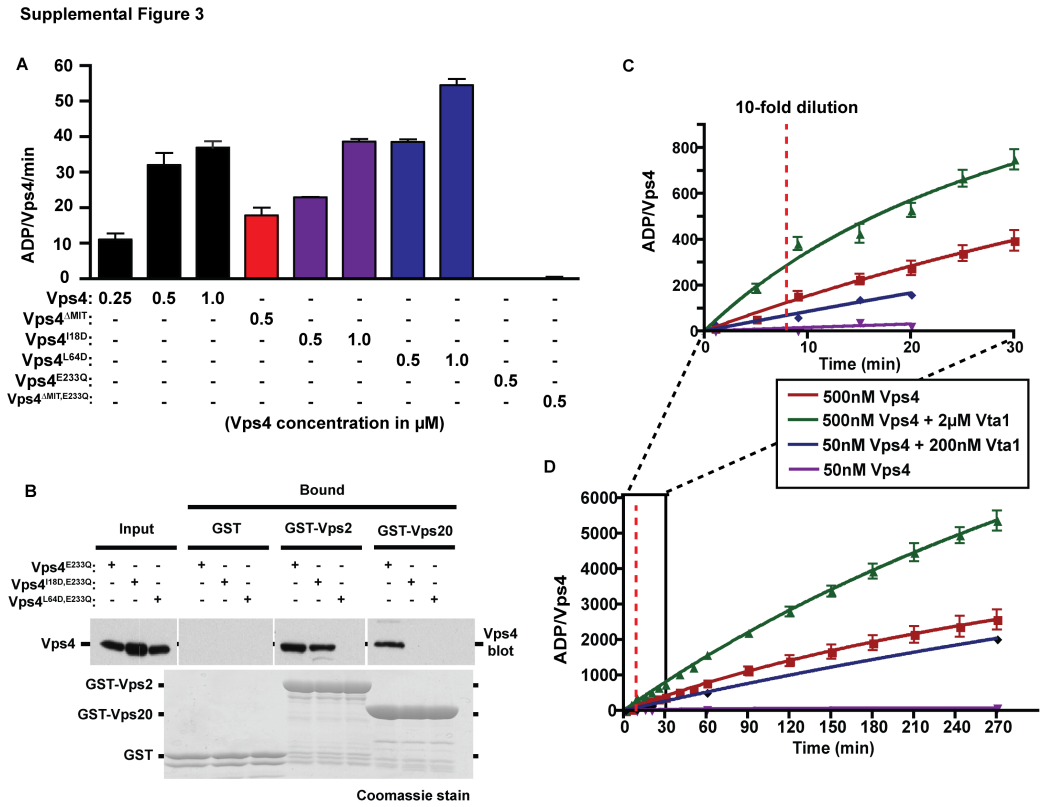

Supplementary Figure 3. Additional biochemical characterization of Vps4. (**A**) ATPase activities (ADP generated/Vps4/min) of wild type Vps4, Vps4$^{\Delta MIT}$, Vps4^{L64D}, Vps4^{I18D}, Vps4^{E233Q} and Vps4$^{\Delta MIT,E233Q}$. (**B**) Two discrete surfaces of the Vps4 MIT domain have been proposed to mediate interactions with distinct MIMs present in Vps2, Did2, and Ist1 (MIM1) and in Vps20, Ist1 and Snf7 (MIM2) (Agromayor et al., 2009; Bajorek et al., 2009a; Kieffer et al., 2008; Obita et al., 2007; Shestakova et al., 2010; Stuchell-Brereton et al., 2007). Mutation of the MIM2 interacting surface of mammalian Vps4A (Vps4A^{V13D}) compromises its interaction with the CHMP6/Vps20 MIM2 without disrupting interaction with CHMP1B/Did2 MIM1 (Kieffer et al., 2008); similarly, a mutation of the MIM1 interacting surface of Vps4A (VPS4A^{L64D}) abrogated CHMP1B/Did2 MIM1 binding while only partially reducing CHMP6/Vps20 MIM2 interaction (Kieffer et al., 2008). Mutations were generated in yeast Vps4 (Vps4^{I18D}, Vps4^{L64D}) to similarly disrupt MIM-MIT interactions. GST, GST-Vps2 (MIM1-containing) or GST-Vps20 (MIM2-containing) affinity purification experiments were performed with Vps4^{E233Q}, Vps4^{I18D,E233Q} [predicted to perturb MIM2 binding specifically (Wes Sundquist and Jack J. Skalicky, University of Utah, personal communication)] and Vps4^{L64D,E233Q} [predicted to disrupt MIM1 binding and partially perturb MIM2 binding (Kieffer et al., 2008)]. Western blotting for Vps4 was performed. Vps4^{E233Q} isolation was evident with both GST-Vps2 and GST-Vps20. While Vps4^{I18D,E233Q} was isolated as predicted with GST-Vps2 but not with GST-Vps20, Vps4^{L64D,E233Q} isolation with GST-

Vps20 was not detected under the conditions utilized. Complementation analysis of *vps4*Δ MVB sorting defects by $vps4^{I118D}$ and $vps4^{L64D}$ is presented in Shestakova *et al.* (2010). (**C, D**) Reactions containing 500nM Vps4 (red), 500nM Vps4 with 2μM Vta1 (green), 50nM Vps4 (purple), and 50nM Vps4 with 200nM Vta1 (blue) were initiated with the addition of ATP to 1mM. The 500nM Vps4 and 500nM Vps4 with 2μM Vta1 reactions were diluted 10-fold 10 minutes after initiation. ATP hydrolysis was assessed both prior to and subsequent to dilution. Data are presented as ADP generated per Vps4 for the 0-30 minute (**A**) and 0-270 minute (**B**) time frames.

Supplement Figure 4

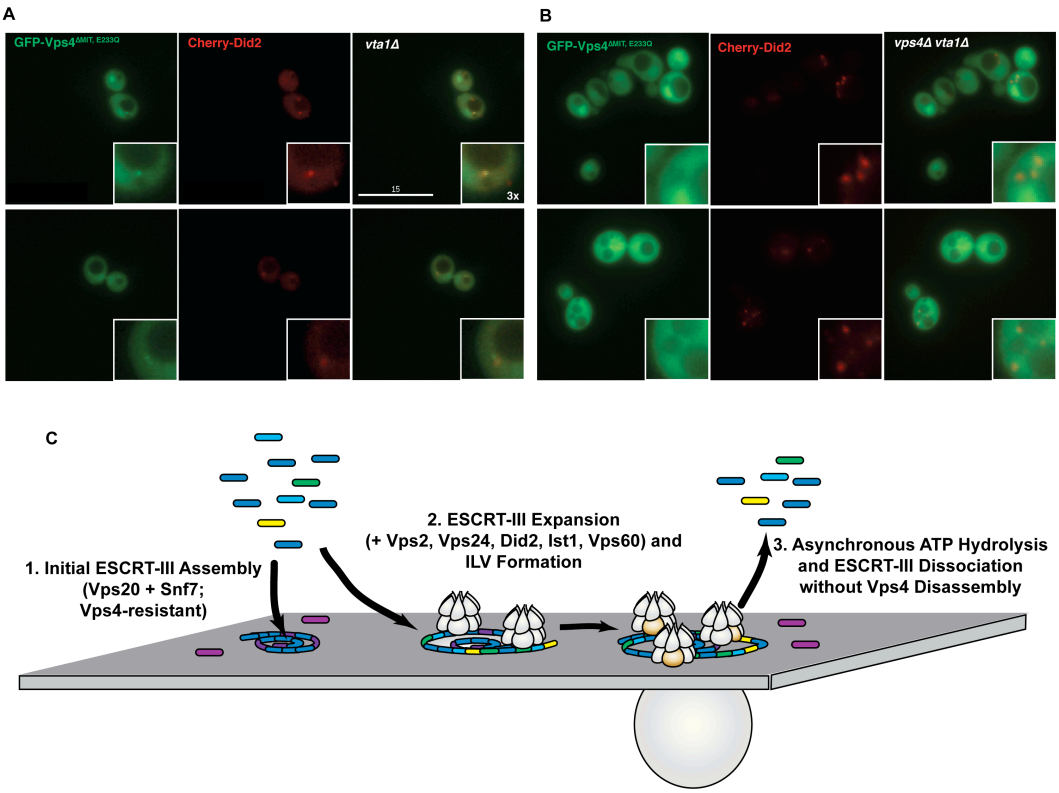

Supplementary Figure 4. Examination of GFP-Vps4$^{\Delta MIT,E233Q}$ localization. Live cell microscopy was performed with *vta1*Δ (A) or *vps4*Δ *vta1*Δ yeast (B) expressing GFP-Vps4$^{\Delta MIT,E233Q}$ (green) and Cherry-Did2 (red), as in Figure 5C, D**. (A)** In *vta1*Δ cells, Cherry-Did2 localizes diffusely throughout the cytosol as well as to peri-vacuolar punctate structures, likely endosomes where MVB sorting occurs. This distribution is consistent with the continued activity of Vps4 in *vta1*Δ cells. GFP-Vps4$^{\Delta MIT,E233Q}$ distribution in these *vta1*Δ cells is similar to Cherry-Did2 with diffuse cytosolic distribution and peri-vacuolar punctate accumulation that co-localizes with Cherry-Did2 (magnified 3x in the inset). (**B**) In the *vps4*Δ *vta1*Δ cells, distinct distributions of Cherry-Did2 and GFP-Vps4$^{\Delta MIT,E233Q}$ are apparent. In the absence of Vps4, Cherry-Did2 punctate association is enhanced. These punctate structures are also Vps24-GFP positive (Figure 5A). By contrast, GFP-Vps4$^{\Delta MIT,E233Q}$ association with Did2-positive structures is no longer apparent in *vps4*Δ *vta1*Δ cells (magnified 3x in the inset). These observations suggest that GFP-Vps4$^{\Delta MIT,E233Q}$ association with the ESCRT-III endosome is dependent on Vps4 and are consistent with GFP-Vps4$^{\Delta MIT,E233Q}$ hetero-oligomerization with Vps4. (**C**) Vps4 is functionally stable in vitro, suggesting that Vps4 functions as a stable oligomer during ESCRT-III disassembly in vivo. Assembly of ESCRT-III appears to initially occur through recruitment and polymerization of Vps20 and Snf7 (**1**). While MIM2 elements may permit Vps4 recruitment to the Vps20-Snf7 polymer, Vps4-mediated disassembly of ESCRT-III appears to require the additional recruitment of the MIM1-containing subunits Vps2, Vps24 and Did2 (**2** and **3**). Vps4-mediated disassembly

does not require dissociation of Vps4 itself nor a full complement of MIT domains nor concerted hydrolysis by all of the subunits within the oligomer. These observations suggest that the Vps4 oligomer may disassemble ESCRT-III polymers in a processive manner. Whether this Vps4 activity is strictly limited to ESCRT-III disassembly subsequent to ILV formation to permit subunit recycling (as depicted) or if Vps4-mediated ESCRT-III remodeling may also actively contribute to ILV formation (transition from **2** to **3**) is a question that remains unresolved. This model does not address additional factors in vivo that regulate recruitment and assembly of the Vps4 subunits or that modulate stability of the Vps4 oligomer; moreover, many aspects of ESCRT-III assembly and Vps4-mediated disassembly depicted here are unsubstantiated and represent artistic license in attempting to depict the concepts discussed above.